Applied Catalysis B: Environmental 108–109 (2011) 39–46

Contents lists available at ScienceDirect

Applied Catalysis B: Environmental

journal homepage: www.elsevier.com/locate/apcatb

Sintering-resistant and self-regenerative properties of Ag/SnO_2 catalyst for soot oxidation

Ken-ichi Shimizu[a,*], Makoto Katagiri[b], Shigeo Satokawa[c], Atsushi Satsuma[b]

[a] Catalysis Research Center, Hokkaido University, N-21, W-10, Sapporo 001-0021, Japan
[b] Department of Molecular Design and Engineering, Graduate School of Engineering, Nagoya University, Nagoya 464-8603, Japan
[c] Department of Materials and Life Sciences, Seikei University, Musashino, Tokyo 180-8633, Japan

ARTICLE INFO

Article history:
Received 18 April 2011
Received in revised form 5 July 2011
Accepted 3 August 2011
Available online 10 August 2011

Keywords:
Soot oxidation
Sintering
Silver
Tin oxide

ABSTRACT

Key factors controlling the thermal and redox-cycle stability of Ag/SnO_2 catalyst were investigated to establish the design concept of "self-regenerative" soot oxidation catalysts. The effect of thermal aging (in air at 1000 °C) on the soot oxidation activity was tested for Ag catalysts supported on SnO_2, CeO_2, ZrO_2, TiO_2, and MgO and SnO_2-supported Cu, Pd, Rh, Ru, and Pt. Ag/SnO_2 is found to be the most effective catalysts in terms of both activity and thermal stability. XRD and EXAFS results showed that particle growth of metal or metal oxide by the thermal aging was the main reason of the decreased soot oxidation activity, and the supported Ag species on Ag/SnO_2 showed high sintering-resistance owing to the Ag–O–Sn bonds at metal–support interface. The effect of redox aging at 800 °C on the soot oxidation activity and structure of Ag/SnO_2 was also studied. H_2-reduction of Ag/SnO_2 lead to the formation of the large (20 nm) particles of Ag_3Sn, which were then redispersed by the reoxidation treatment to small Ag nanoparticles. This self-regenerative property lead to no catalyst deactivation of Ag/SnO_2 after successive redox treatments. It is concluded that the strong chemical interaction between silver and tin species (metallic and oxidic Sn) under both reductive and oxidative environments at high-temperature enables the design of highly sintering resistant Ag-based oxidation catalysts.

1. Introduction

The development of platinum-group-metal (PGM)-free automotive catalysts with high durability is one of the most important goal in the research of environmental catalysis [1]. Although it is recently established that nanoparticles of Au [2,3] and Ag [4,5] can be promising candidates of PGM-free oxidation catalysts, a significant barrier to their practical use is their tendency to agglomerate at lower temperature (typically 600 °C) than PGM, which results in an irreversible catalyst deactivation [3,5]. Supported PGM nanoparticles in the conventional automotive catalysts sinter during high-temperature oxidation/reduction cycles typically encountered in automotive exhaust gas [1]. Recently, highly durable PGM-based three-way catalyst, such as perovskite-supported Pd [7] and ceria-supported Pt [6,8] were developed and commercialized. In these catalysts, cationic PGM species are stabilized under the high-temperature oxidative condition, by forming a solid solution with the perovskite structure or rigid Pt–O–Ce bonds, which prevents metal particle growth. If we design a new PGM-free catalyst, in which active metal species have a strong interaction with a support under reductive as well as oxidative environments at high-temperature leading to reversible regeneration of the active site structure, the developed catalyst may be highly durable and inexpensive. Previous fundamental studies suggest that reversible structural changes of active metal species during redox cycles should be a key to design a sintering-resistant catalyst [1,6–9].

Strong chemical interaction between tin oxide (SnO_2) and PGM (Pd [10,11], Pt [12–14], and Ru [15]) has been extensively studied by Eguchi and co-workers. In spite of the smaller surface area (<10 $m^2\,g^{-1}$) than conventional support such as Al_2O_3, a few nanometer-sized PGM nanoparticles dispersed on SnO_2 were prepared by a conventional impregnation method followed by calcination. They also studied nanoscopic observation of sintering and redispersion phenomena of Pt/SnO_2 [13,14]. The H_2-reduction of Pt/SnO_2 leads to the formation of large particles of intermetallic compounds (PtSn, Pt_3Sn). These large particles were redispersed by the reoxidation treatment to the Pt nanoparticles with similar size to the as-prepared catalyst. However, the redispersed catalyst showed lower CO oxidation activity than the as-prepared one [14]. We hypothesized that these phenomena can be used to design a sintering-resistant "self-regenerative" silver catalyst.

The use of catalytic filters is one of the alternatives to avoid diesel soot particle (small-size carbon particle) being emitted to the atmosphere [16]. The catalyst supported on the filter must be

* Corresponding author. Tel.: +81 11 706 9240; fax: +81 11 706 9163.
E-mail address: kshimizu@cat.hokudai.ac.jp (K.-i. Shimizu).

0926-3373/$ – see front matter © 2011 Elsevier B.V. All rights reserved.
doi:10.1016/j.apcatb.2011.08.003

active within the exhaust gas temperatures (300–400 °C) in order to regenerate the filter continuously, thus avoiding an increment in the pressure drop that could lead to engine failure. However, under certain conditions such as when a large amount of soot is accumulated on the catalytic filter, a reaction runaway could occur thus reaching high temperatures, which could lead to catalyst deactivation and additional failure of the catalyst-filter system [17]. Therefore, the catalyst must have thermal and redox stability under the combustion exhaust environment. Among various catalyst reported to date, including metal oxides [16,18,19] and precious metals [16,20–25], a silver-loaded ceria is the promising catalyst for low temperature soot oxidation [21–25], though it significantly deactivates due to metal sintering [24].

In this paper we investigated soot oxidation activity and thermal and redox-cycle stability of silver-loaded metal oxides and metal-loaded SnO_2 catalysts. Combined with characterization results, key factors controlling the activity and durability of Ag/SnO_2 are investigated, and a sintering inhibition mechanism is discussed to establish the design concept of durable soot oxidation catalysts.

2. Experimental

2.1. Catalyst preparation

H_2SnO_3 (Kojundo Chemical Laboratory Co., Ltd.), CeO_2 (HSA 1A, Rhodia Electronics Catalysis, 157 $m^2\,g^{-1}$), and MgO (1000A, Ube Material Industries, Ltd.) were commercially purchased. $ZrO_2{\cdot}nH_2O$ was prepared by hydrolysis of zirconium oxynitrate 2-hydrate in distilled water by gradually adding an aqueous NH_4OH solution (1.0 mol dm^{-3}), followed by filtration of precipitate, washing with distilled water three times, and dryness at 100 °C. Silver-loaded metal oxides were prepared by impregnating the support materials (H_2SnO_3, CeO_2, MgO, $ZrO_2{\cdot}nH_2O$) with an aqueous solution of silver nitrate followed by evaporation to dryness at 60 °C, calcination in air at 600 °C for 1 h. Metal-loaded SnO_2 catalysts, M/SnO_2 (M = Cu, Pd, Rh, Ru, Pt; metal loading = 5 wt%), were prepared by impregnating H_2SnO_3 with an aqueous solution of metal nitrate (Cu) or metal chloride (Ru), or nitric acid solution of metal nitrate (Pd, Rh) or $Pt(NH_3)_2(NO_2)_2$, followed by evaporation to dryness at 70 °C, and by calcination in air at 600 °C for 1 h. Catalyst name is designated as M*x*Sn, where *x* is the metal (M) loading (wt%).

2.2. Characterization

X-ray diffraction (XRD) patterns of the powdered catalysts were recorded with a Rigaku MiniFlex II/AP diffractometer with Cu Kα radiation (30 V, 15 mA) at a scanning speed of 1°/min. Average particle size of Ag was calculated from the half-width of the silver peak from the XRD pattern using Scherrer equation. Instead of the most intense Ag(1 1 1) line, a relatively weak (2 0 0) line is used for the analysis, because the former line is close to a line of SnO_2.

In situ XRD measurements were carried out by a Rigaku Ultima IV diffractometer equipped with an in situ cell that allows heating and introduction of gases. To trace the structural changes of the catalyst, 30 mg of a catalyst powder was loaded into the cell and heated up to 700 °C under a flow of Ar (total flow: 100 mL min^{-1}). Then, XRD patterns were recorded from 36.5° to 38.5° at a scanning speed of 2°/min under a flow of 10% H_2/N_2 or air (100 mL min^{-1}).

Ag K-edge XAFS (X-ray absorption fine structure) measurements were performed in transmission mode at the BL01B1 in the SPring-8 (Proposal No. 2008A1633). The storage ring was operated at 8 GeV. A Si(1 1 1) single crystal was used to obtain a monochromatic X-ray beam. Samples were sealed in cells made of polyethylene under ambient atmosphere and XAFS spectra were taken at room temperature. The analyses of the extended X-ray absorption fine structure (EXAFS) and X-ray absorption near-edge structures (XANES) were performed using the REX version 2.5 program (RIGAKU). The Fourier transformation of the k^3-weighted EXAFS oscillation from *k* space to *r* space was performed over the range 40–140 nm^{-1} to obtain a radial distribution function. The inversely Fourier filtered data were analyzed with a usual curve fitting method in the *k* range of 40–140 nm^{-1}. For the curve-fitting analysis, the empirical phase shift and amplitude functions for Ag–Ag and Ag–O shells were extracted from the data for Ag foil and Ag_2O, respectively.

2.3. Catalytic soot oxidation

The catalytic activity for soot oxidation was determined using commercially available carbon black powders (Mitsubishi Chemical Corporation, MA7; surface area 115 $m^2\,g^{-1}$, average particle size 24 nm) as model diesel soot. The soot and catalyst with a weight ratio of 1/20 were ground for 5 min to obtain so-called tight-contact mixtures. The catalytic test was carried out with gravimetric thermal analysis (TG/DTA, Rigaku 8120). The soot/catalyst mixture (10 mg) was heated from room temperature to 600 °C at a rate of 5 °C min^{-1} in a stream of 20% O_2 balanced with N_2 (100 $cm^3\,min^{-1}$). The temperature which gives maximum intensity of the exothermic DTA peak (T_{max}) was used to compare soot oxidation activity of different catalyst. The effluent gas was analyzed by nondispersive infrared CO/CO_2 analyzers (Horiba VIA510).

3. Results and discussion

3.1. Activity and thermal durability of M/SnO_2

Previous works by Eguchi and co-workers have revealed that as-calcined M/SnO_2 catalysts (M = Pt, Pd, Ru) are highly dispersed on the support, because strong chemical interactions between noble metals and SnO_2 occur under oxidizing conditions [10–15]. In the soot oxidation catalyst-filter system, the catalyst must be thermally stable under oxidative atmosphere. Therefore, the effect of high temperature aging in air on the catalytic soot oxidation activity was investigated as the first screening study. To accelerate thermal aging of the catalysts, a relatively severe aging condition (T = 1000 °C, t = 10 h) was adopted. It is important to note that the aging temperature (1000 °C) is higher than the melting point of silver (961 °C). Soot oxidation activity was evaluated by exothermal change in DTA profile. Typical DTA profiles versus reaction temperature are shown in Fig. 1. For the fresh Ag5Sn sample as the standard catalyst in this study, the temperature for the maximum intensity of the exothermic DTA peak (T_{max}) was 366 °C, which was nearly consistent with the temperature for the maximum intensity of the CO_2 emission profile (365 °C). Thus, we used the T_{max} value in DTA profiles as a parameter to compare the soot oxidation activity of different catalysts. The T_{max} values are summarized in Table 1. Among the SnO_2-supported transition metal catalysts calcined at 600 °C (fresh catalysts), T_{max} increased in the order Ag5Sn (366 °C) < Ru5Sn (433 °C) < Rh5Sn (450 °C) < Pt5Sn (451 °C) < Cu5Sn (455 °C) < Pd5Sn (479 °C). As shown in Fig. 1, the heat treatment at 1000 °C for 10 h did not essentially change the DTA profile of Ag5Sn, which indicates a high thermal durability of Ag5Sn. In contrast, Cu5Sn, Pd5Sn and Pt5Sn were not thermally durable; T_{max} values were markedly increased by the heat treatment. Although Ru5Sn and Rh5Sn showed high thermal durability, their T_{max} values after the heat treatment were higher than that of Ag5Sn. Consequently, among the SnO_2-supported transition metal catalysts tested, Ag5Sn is the most effective catalyst in terms of the activity and thermal durability. The effect of support oxides on the activity and durability of silver catalysts was also studied. In our previous study, we reported that Ag/CeO_2 was one of the most

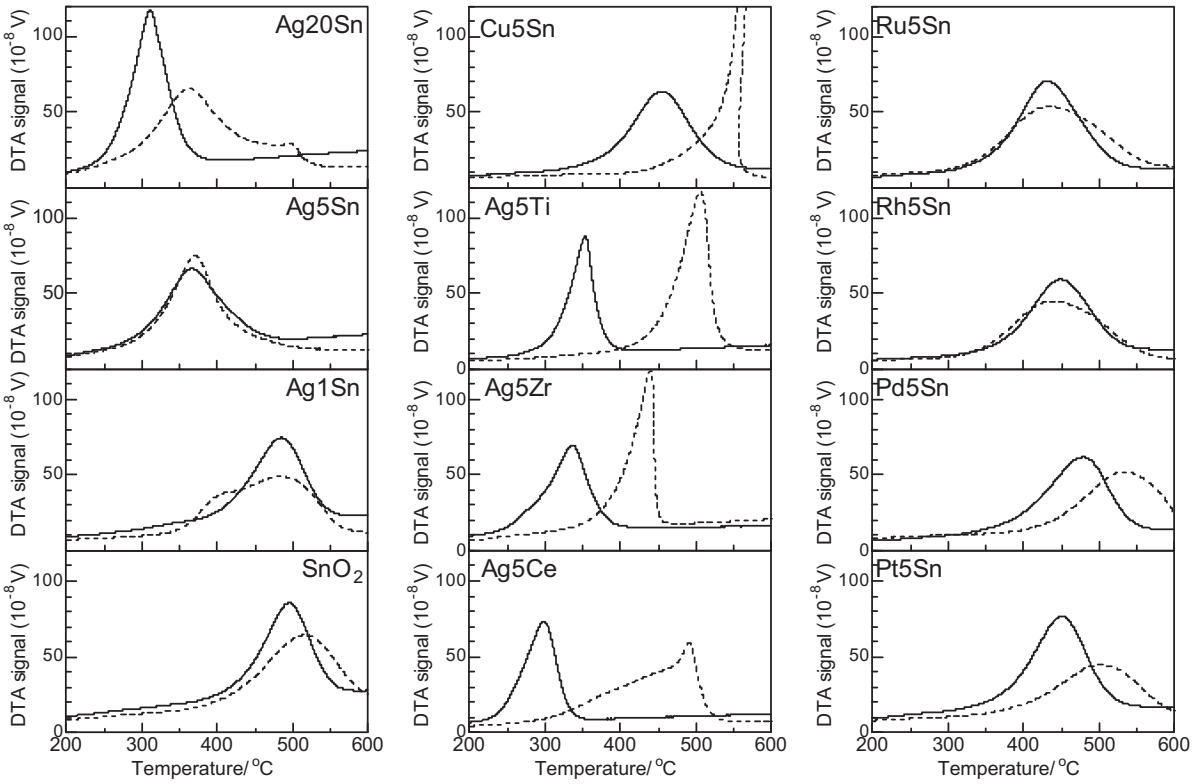

Fig. 1. DTA profiles for carbon oxidation with fresh (—) and aged (--) catalysts. Aged catalysts were heated in air at 1000 °C for 10 h. Carbon oxidation conditions: soot/catalyst = 1/20 (w/w), heating rate = 10 °C min^{-1}, 20% O_2/N_2 flow (100 cm^3 min^{-1}), tight contact.

active catalysts for soot oxidation among various metal oxide catalysts [25]. As expected, among the as-prepared silver catalysts, Ag5Ce showed the highest activity; T_{max} for the fresh silver catalysts increased in the order Ag5Ce (298 °C) < Ag5Zr (336 °C) < Ag5Ti (354 °C) < Ag5Sn (366 °C) < Ag5Mg (437 °C). However, the DTA profile of Ag5Ce shows that the thermal aging at 1000 °C results in a significant deactivation of this catalyst. T_{max} for the aged silver catalysts increased in the order Ag5Sn (370 °C) < Ag5Zr (440 °C) < Ag5Ce (491 °C) < Ag5Ti (506 °C) < Ag5Mg (508 °C). From the above results, it is concluded that Ag5Sn is the most effective soot oxidation catalysts in terms of both activity and thermal durability.

The fresh and aged catalysts were characterized by XRD. The XRD pattern (Fig. 2) of the fresh Ag5Sn catalyst was identical to that of SnO_2, and the diffraction lines ascribed to the silver-containing compounds were absent. This suggests that small silver species are highly dispersed on SnO_2, which will be confirmed by EXAFS in

Table 1
List of 5 wt% Ag/MO_x catalysts after aging in air at 1000 °C for 10 h.

Samples	Phase	D/nm[a]	D_{SnO2}/ nm[b]	T_{max}/°C[c]
Ag5Sn	Ag metal	11	27	370 (366)
Rh5Sn	–	–	21	443 (450)
Ru5Sn	–	–	24	434 (433)
Pt5Sn	Pt metal	31	26	503 (451)
Pd5Sn	PdO	16	28	530 (479)
Cu5Sn	CuO	34	28	588 (455)
Ag5Ce	Ag metal	20	–	491 (298)
Ag5Zr	Ag metal	18	–	440 (336)
Ag5Ti	Ag metal	27	–	506 (354)
Ag5Mg	Ag metal	37	–	508 (437)

[a] Average size of metal or metal oxide particle estimated from XRD analysis.
[b] Average size of SnO_2 particle estimated from XRD analysis.
[c] The temperature for the maximum intensity of the exothermic DTA peak (T_{max}). T_{max} values for the fresh catalysts (before aging) are in parentheses.

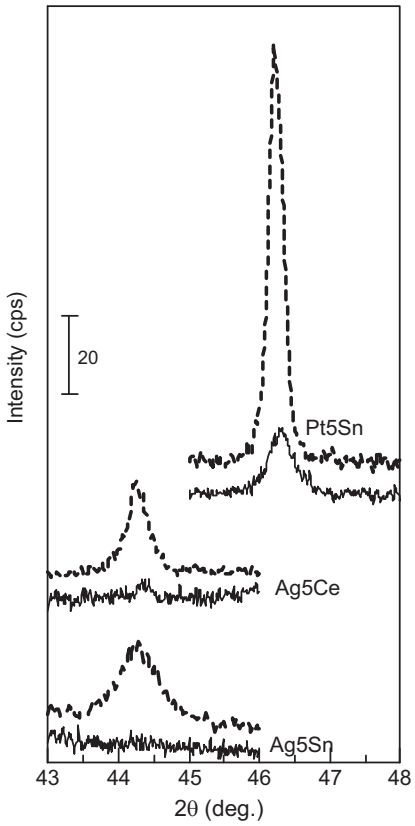

Fig. 2. XRD patterns of fresh (—) and aged (--) catalysts. Aged catalysts were heated in air at 1000 °C for 10 h.

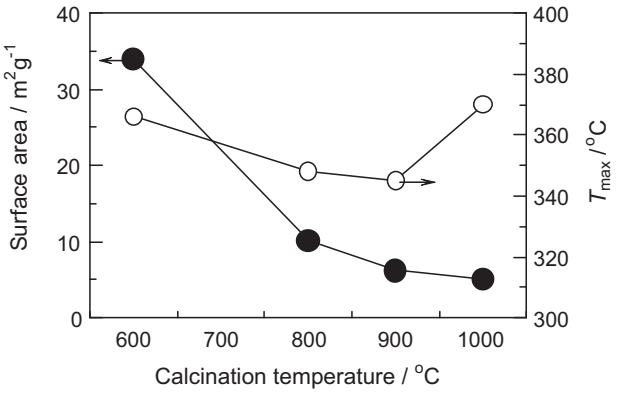

Fig. 3. Plots of (○) T_{max} for carbon oxidation and (●) catalyst surface area vs calcination temperature of Ag5Sn. Calcination time was 1 h.

the following section. In the XRD pattern of the aged Ag5Sn, there is a Ag (2 0 0) diffraction line at 44.3°. Table 1 includes the average particle size of metal or metal oxide species calculated from the half-width of the peak using Scherrer equation. The Ag particle size of the aged Ag5Sn (11 nm) was smaller than those of the aged Ag5Ce, Ag5Zr, Ag5Ti and Ag5Mg catalysts (18–37 nm). XRD patterns of the aged Rh5Sn and Ru5Sn were basically identical to that of SnO_2, indicating highly dispersed states of Rh and Ru species on SnO_2. In contrast, the aged Pt5Sn showed a large diffraction line due to metallic Pt (Fig. 2), and particle size of Pt was estimated to be 31 nm. XRD results of aged Cu5Sn and Pd5Sn showed the presence of large CuO (34 nm) and PdO (16 nm) particles. Summarizing the above results, the following conclusion can be drawn. Particle growth of metal or metal oxide by the thermal aging is the main reason of the decreased soot oxidation activity. The supported metal species in Ag5Sn, Rh5Sn and Ru5Sn catalysts shows higher sintering-resistance than other catalysts, which results in a lower level of catalyst deactivation after the treatment at 1000 °C for 10 h. Strong chemical interaction between precious metals with SnO_2 support under oxidizing condition, reported by Eguchi and coworkers, may be the reason of high sintering-resistance of Ag5Sn, Rh5Sn and Ru5Sn. The origin of the interaction between Ag and SnO_2 is discussed in the following section.

3.2. Structure–activity relationship for soot oxidation by Ag/SnO_2

The effect of calcination temperature on the surface area and the activity of Ag5Sn is shown in Fig. 3. With increase in the temperature from 600 to 900 °C, the surface area monotonically decreased from 34 to 6.2 m^2 g^{-1}. In spite of the decrease in the surface area, T_{max} for soot oxidation decreased from 366 to 345 °C.

As shown in Fig. 2, XRD pattern of the fresh Ag/SnO_2 samples showed no diffraction lines due to silver and silver oxides. The structure of the X-ray amorphous species can be investigated with XAFS, because it potentially provides an average structural information of all the Ag species in the sample. Fig. 4A shows the Fourier transforms of the k^3-weighted Ag K-edge EXAFS of Ag/SnO_2 catalysts with various Ag loading (1, 5, 10, 20 wt%). The structural parameters derived from curve-fitting analysis are listed in Table 2. The EXAFS of Ag1Sn consists of a Ag–O contribution at bond distance of 2.12 Å with coordination number (N_{Ag-O}) of 1.0 and a weak Ag–Ag contribution (N_{Ag-Ag} = 0.6) due to metallic Ag. Fig. 4B shows Ag K-edge XANES spectra, which are known to be sensitive to the oxidation state of X-ray absorbing atom. The XANES spectrum of $AgNO_3$, as a reference compound of ionic Ag^+ species, showed a peak around 25515 eV characteristic to ionic Ag^+ species [26]. XANES spectrum of Ag1Sn showed the peak due to the ionic Ag^+ species. The EXAFS and XANES results indicate that highly

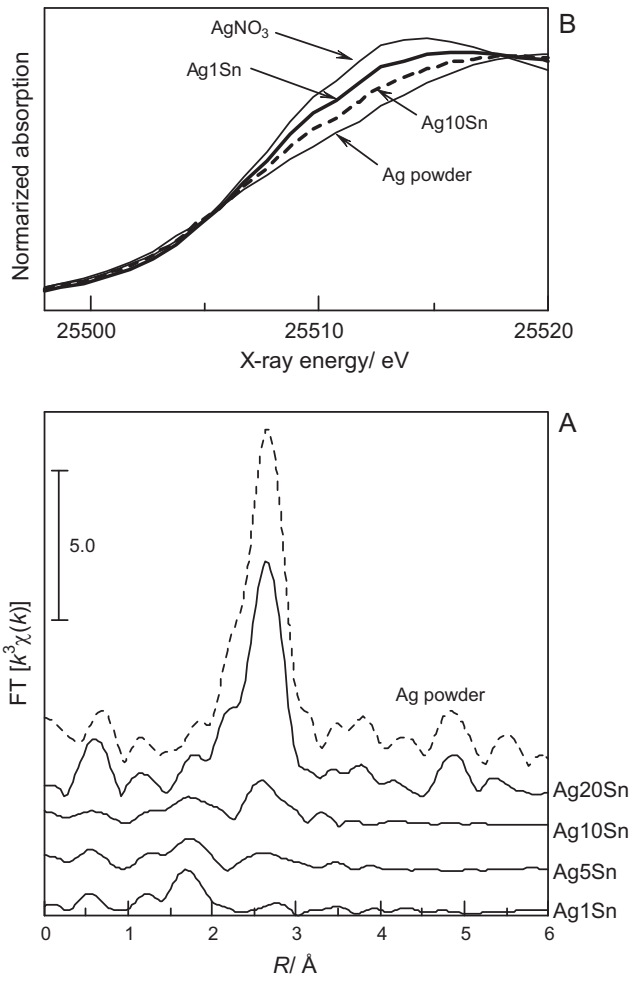

Fig. 4. Ag K-edge EXAFS Fourier transforms (A) and XANES spectra (B) of fresh Ag*x*Sn catalysts and reference compounds.

dispersed Ag^+ species are the dominant Ag species in Ag1Sn. The Ag–O bond distance (2.12 Å) is longer than that of Ag_2O (2.04 Å). The most probable model can be the Ag^+ ion anchored by the surface oxygen atoms of SnO_2 support by forming a Ag–O–Sn bond. The EXAFS spectra of Ag*x*Sn samples (x = 5 and 10 wt%) consist of a Ag–O contribution at bond distance of 2.13–2.14 Å with coordination number (N_{Ag-O}) of 0.7–0.8 and a Ag–Ag contribution at bond distance of 2.81–2.82 Å with coordination number (N_{Ag-Ag}) of 2.2–3.8. The N_{Ag-Ag} value of 2.2–3.8 suggests that the size of Ag

Table 2
Curve-fitting analysis of Ag K-edge EXAFS of Ag/SnO_2.

Ag loading (wt%)	Shell	N[a]	R/Å[b]	σ/Å[c]	R_f/%[d]
Ag5Sn	Ag	2.2	2.81	0.113	7.5
	O	0.8	2.14	0.105	
Ag5Sn–O	Ag	4.7	2.84	0.099	4.8
	O	0.4	2.13	0.070	
Ag5Sn–OR	Ag	11.9	2.95	0.087	1.0
Ag5Sn–ORO	Ag	9.7	2.89	0.071	0.6
Ag1Sn	Ag	0.6	2.89	0.087	8.7
	O	1.0	2.12	0.093	
Ag10Sn	Ag	3.8	2.82	0.101	2.7
	O	0.7	2.13	0.110	
Ag20Sn	Ag	9.9	2.89	0.067	0.7

[a] Coordination numbers.
[b] Bond distance.
[c] Debye–Waller factor.
[d] Residual factor.

metal cluster is quite small. Taking this fact into account, the Ag–O bond observed in these catalysts could be due to the Ag–O–Sn bond at cluster–support interface. The Ag20Sn sample shows a Ag–Ag contribution at bond distance of 2.89 Å with coordination number of 9.9. The Ag–Ag bond distances of Ag20Sn is consistent with that of bulk silver (2.89 Å), while N_{Ag-Ag} is lower than that of bulk silver (CN_{Ag-Ag} = 12), suggesting that metallic Ag species in Ag20Sn are small nanoparticles. To estimate the effect of Ag loading on the relative amount of the metallic silver and ionic Ag^+ species, the coordination numbers, N_{Ag-O} and N_{Ag-Ag}, are plotted as a function of the loading in Fig. 5B. With increase in the silver loading, N_{Ag-O} decreased and N_{Ag-Ag} increased, indicating that the relative amount of the metallic Ag species with respect to the Ag^+ species increased with silver loading. The result of XANES (Fig. 4B) supports this model; the intensity of the peak around 25515 eV due to Ag^+ species decreases with Ag loading.

The DTA curves for soot oxidation by Ag*x*Sn catalysts are shown in Fig. 1. The fresh Ag1Sn catalyst showed nearly identical DTA profile to SnO_2. As shown in Fig. 5A, T_{max} of the fresh catalysts decreased with silver loading. Taking into account the result that relative amount of the metallic Ag species with respect to the Ag^+ species increased with silver loading. Fig. 5 shows that the catalytic activity of Ag*x*Sn increases with increase in the Ag loading. It is concluded that metallic Ag is active species for soot oxidation, while highly dispersed Ag^+ ion anchored by the surface oxygen atoms of SnO_2, as the predominant Ag species in Ag1Sn, is catalytically inactive.

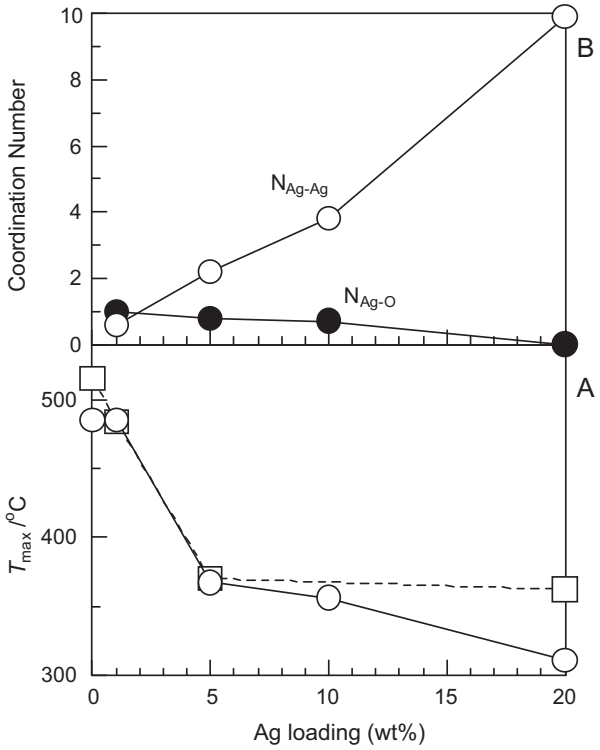

Fig. 5. (A) T_{max} for carbon oxidation for fresh (—) and aged (–-) Ag5Sn catalysts and (B) coordination numbers for the fresh Ag5Sn as a function of Ag loading. Aged catalysts were heated in air at 1000 °C for 10 h.

3.3. Redox aging of Ag/SnO_2

In the catalytic soot filter for the practical application, a large amount of soot can be accumulated in the filter, which leads to a reaction runaway. The catalytically active metal nanoparticles can be sintered under a locally reductive atmosphere at high temperature, which would lead to catalyst deactivation and additional failure of the catalyst-filter system. To obtain design concept for soot oxidation catalysts with high redox durability, we studied the effect of high temperature redox aging on the soot oxidation activity and structure of Ag5Sn. Table 3 summarizes the structure and soot oxidation activity of Ag5Sn catalysts after

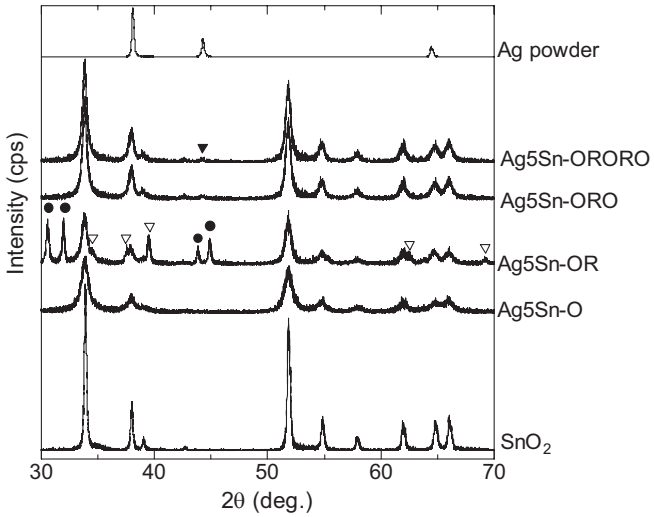

Fig. 6. XRD patterns of Ag5Sn after successive redox treatments at 800 °C: (

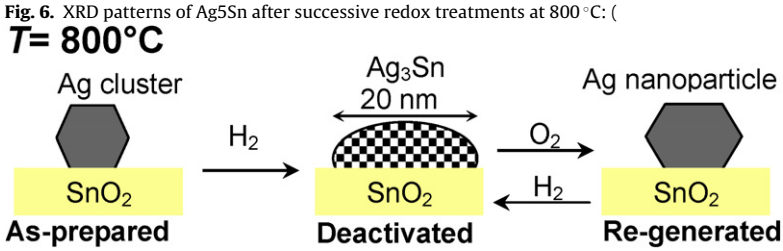

) Ag_3Sn, (●) Sn, (▼) Ag.

Table 3
List of 5 wt% Ag/SnO_2 catalysts after redox aging treatments at 800 °C.

Sample name	Pre treatment	$S_{BET}/m^2\ g^{-1}$	Phase (XRD)	T_{max}/°C
Ag5Sn	As-prepared (calcined at 600 °C)	34	–	366
Ag5Sn	Oxidation of Ag5Sn	18	–	348
Ag5Sn	Reduction of Ag5Sn–OR	19	Ag_3Sn, Sn	489
Ag5Sn	Oxidation of Ag5Sn–ORO	14	Ag	345
Ag5Sn	Reduction and oxidation of Ag5Sn–ORO	12	Ag	347

[a] Oxidation was conducted in 10%O_2/He at 800 °C for 10 min.
[b] Reduction was conducted in 1%H_2/He at 800 °C for 10 min.

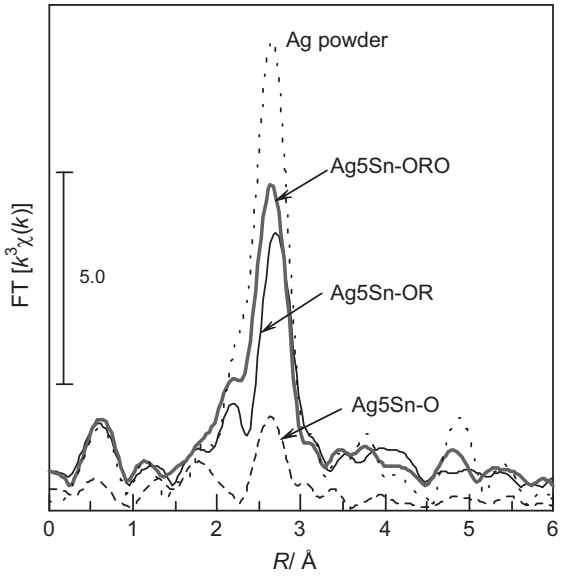

Fig. 7. Ag K-edge EXAFS Fourier transforms (A) and XANES spectra (B) of Ag5Sn samples a after successive redox treatments at 800 °C.

aging treatments at 800 °C. XRD patterns of Ag5Sn catalysts after successive redox treatments are shown in Fig. 6. XRD result of the Ag5Sn sample after high temperature treatment in oxidizing condition (10% O_2), named Ag5Sn–O, showed no diffraction lines due to metallic Ag particle. Fig. 7 shows Fourier transforms of EXAFS for a series of Ag5Sn samples, and the structural parameters from the EXAFS data are included in Table 2. Compared with the as-prepared Ag5Sn, Ag5Sn–O showed larger N_{Ag-Ag}. This suggests that the heat treatment increases the relative amount of the Ag metal clusters with respect to the Ag(I) species as well as an increase in the size of Ag metal clusters. The Ag–Ag coordination number of Ag5Sn–O (N_{Ag-Ag} = 4.7) is still much smaller than that of bulk Ag metal (N_{Ag-Ag} = 12), which indicates that small Ag clusters are dominant Ag species. This result shows that Ag clusters supported on SnO_2 did not markedly sinter under oxidizing condition at 800 °C. A residual Ag–O contribution (N_{Ag-O} = 0.4 at 2.13 Å) suggests that the Ag–O–Sn bond at cluster–support interface are stable even under the high-temperature oxidative environment. From these results, we propose that the formation of Ag–O–Sn bonds at the metal–support interface is responsible for the high sintering resistance of the Ag/SnO_2 catalyst under high-temperature oxidizing condition.

Then, Ag5Sn–O was reduced in 1% H_2 at 800 °C to yield the sample named Ag5Sn–OR. In the XRD pattern of Ag5Sn–OR, lines due to the intermetallic compound (Ag_3Sn) and Sn metal particle were observed, but lines due to Ag metal were absent. The particle size of Ag_3Sn was 20 nm. The EXAFS of Ag5Sn–OR was fitted by a Ag–M (M = Ag or Sn) shell (Table 2). The empirical phase shift and amplitude functions extracted from the data for Ag foil were used for the curve-fitting analysis. The interatomic distance (R_{Ag-M} = 2.95 Å) was nearly consistent with that for the crystallographic data of bulk Ag_3Sn (R_{Ag-M} = 2.93–2.98 Å) [27]. These results indicate that Ag_3Sn is the predominant silver species in Ag5Sn–OR. The reduced catalyst was then heated in oxidizing condition (10% O_2) at 800 °C. The XRD pattern of the reoxidized catalyst, Ag5Sn–ORO, was basically identical to that of SnO_2. The EXAFS of Ag5Sn–ORO consists of a Ag–Ag shell with N_{Ag-Ag} of 9.7 at R_{Ag-M} of 2.89 Å, which indicates that Ag metal nanoparticle is the predominant silver species in this sample. Following the method by Jentys [28], average size of Ag metal nanoparticle estimated with the N_{Ag-Ag} value was 2.6 nm. Summarizing these results, the schematic model of the structural changes during the successive oxidation/reduction/reoxidation treatments is shown in Fig. 8. The soot oxidation experiments were also carried out for a series of Ag5Sn catalysts, and T_{max} values are shown in Fig. 8 and Table 3. Fig. 9 shows DTA profiles for representative catalysts. The high temperature (800 °C) treatment of the as-prepared Ag5Sn in O_2 increases the relative amount of the Ag metal clusters with respect to the ionic Ag–O–Sn species at cluster–support interface, which results in a slight increase in the catalytic activity. After the subsequent treatment in reductive atmosphere at 800 °C (Ag5Sn–OR), the Ag cluster is completely converted to the intermetallic compound (Ag_3Sn) with large particle size (20 nm), which is inactive for soot oxidation. However, the activity of the completely deactivated catalyst is recovered by the subsequent reoxidation treatment, because Ag_3Sn is completely converted to Ag nanoparticles as active species. The Ag5Sn–ORORO catalyst, prepared by the second reduction/reoxidation treatment of Ag5Sn–ORO at 800 °C, shows the T_{max} (347 °C) value comparable to that of Ag5Sn–ORO (345 °C), indicating that the "self-regeneration" phenomena is reversible. It is important to note that the regeneration of the soot oxidation activity after the successive oxidation/reduction/reoxidation treatment at 800 °C was not observed for Ag5Ce, Ag5Zr, Ag5Ti, and Ag5Mg samples, and large Ag metal particles with size in the range

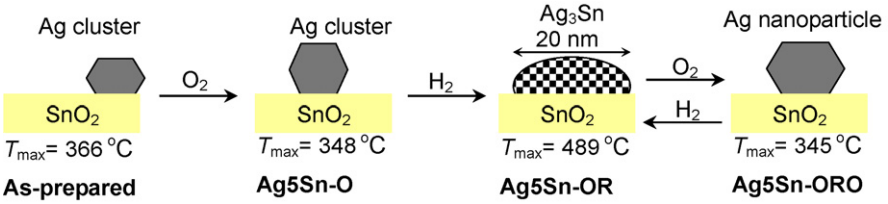

Fig. 8. Schematic pictures of structural changes of Ag/SnO_2 during redox aging.

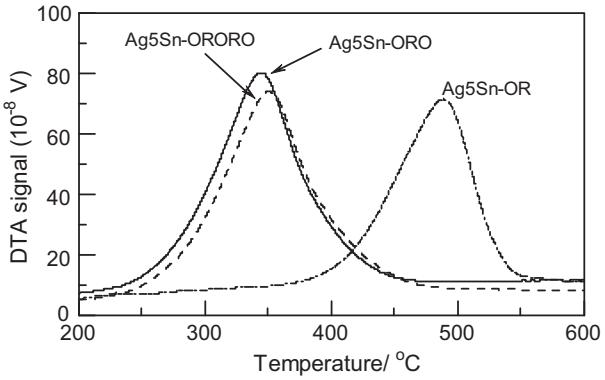

Fig. 9. DTA profiles for carbon oxidation with Ag5Sn catalysts. Conditions: soot/catalyst = 1/20 (w/w), heating rate = 10 °C min^{-1}, 20% O_2/N_2 flow (100 cm^3 min^{-1}), tight contact.

15–37 nm were observed in these catalysts after the aging. Considering the XRD result that intermetallic compounds were not observed for these catalysts after reduction at 800 °C, it can be concluded that the formation of the intermetallic compound (Ag_3Sn) is responsible for the self-regenerative function of the Ag/SnO_2 catalyst.

To obtain a direct evidence for the dynamic structural change illustrated in Fig. 8, we carried out in situ XRD observation during redox treatment at 700 °C. The Ag20Sn catalyst calcined at 800 °C was adopted as a test sample. The catalyst, heated at 700 °C in a flow of Ar, was exposed to a flow of 10% H_2/N_2 for 4 min, and then to Ar(1000 mL min^{-1}) for 1 min, and then to a flow of air. The XRD patterns recorded during this redox treatment were shown in Fig. 10. It was found that the H_2-reduction for 4 min resulted in the conversion of Ag metal (37.6°) to Ag_3Sn. When the reduced catalyst was exposed to oxidizing atmosphere, Ag_3Sn was converted to Ag metal within 4 min.

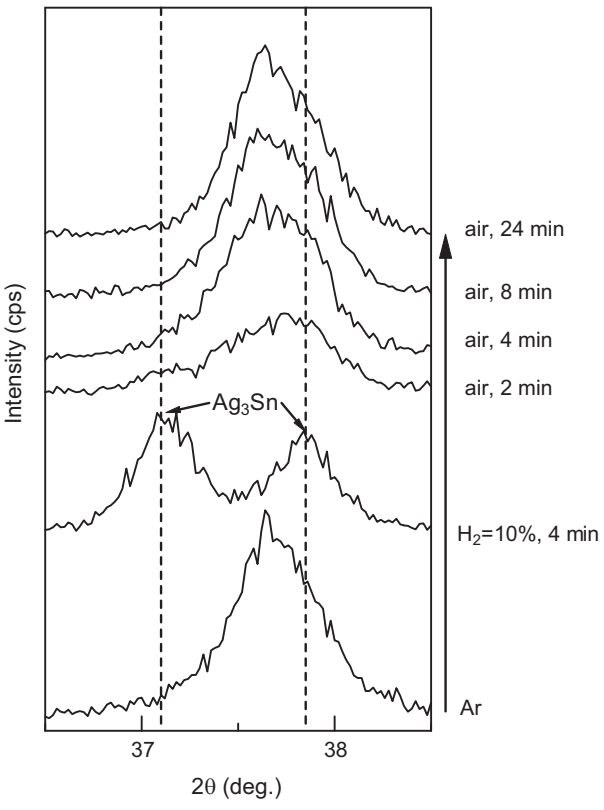

Fig. 10. In situ XRD patterns of Ag20Sn catalyst during successive redox treatments at 700 °C.

The redispersion phenomena of Ag/SnO_2 is quite similar to that reported by Eguchi and co-workers for Pt/SnO_2 catalyst [13,14]. Large particles of intermetallic compounds (PtSn, Pt_3Sn) were formed by H_2-reduction of Pt/SnO_2 at 400 °C, which were redispersed by the reoxidation treatment at 400 °C to the Pt nanoparticles with similar size to the as-prepared catalyst. However, the reoxidized Pt/SnO_2 catalyst showed lower CO oxidation activity than the as-prepared one [14]. Our results clearly show that this strategy is effective for the design of the sintering-resistant and self-regenerative automotive catalyst.

4. Conclusions

Among various metals (Ag, Cu, Pd, Pt, Rh, and Ru) supported on SnO_2, Ag/SnO_2 showed highest soot oxidation activity. Ag/SnO_2 did not markedly sinter under oxidizing condition at 1000 °C, which is higher than the melting point of silver (961 °C). For SnO_2-supported Cu, Pd, and Pt and Ag particles on CeO_2, ZrO_2, TiO_2, and MgO, metal or metal oxide particles sintered, resulting in catalyst deactivation. In contrast, small Ag clusters, stabilized by Ag–O–Sn bonds at cluster–support interface, were preserved after the treatment under oxidizing condition at 800 °C. The effect of high-temperature (800 °C) redox-cycle on the soot oxidation activity and structure of Ag/SnO_2 showed that the large Ag_3Sn particles once formed during reductive condition were redispersed to Ag metal nanoparticles under oxidizing conditions. Owing to this self-regenerative property, Ag/SnO_2 did not deactivate after the successive redox treatments. It is proposed that the strong chemical interaction between Ag and Sn (or SnO_2) under both reductive and oxidative environments at high-temperature enables the design of highly sintering resistant Ag-based oxidation catalysts for soot oxidation.

Acknowledgments

This work was supported by the Japanese Ministry of Education, Culture, Sports, Science and Technology via Grant-in-Aids for Scientific Research B (20360361) and for Young Scientists A (22686075). The X-ray absorption experiment was performed with the approval of the Japan Synchrotron Radiation Research Institute (Proposal No. 2008A1633).

References

[1] A. Cao, R. Lu, G. Veser, Phys. Chem. Chem. Phys. 12 (2010) 13499.
[2] M. Haruta, T. Kobayashi, H. Sano, N. Yamada, Chem. Lett. (1987) 405.
[3] A.A. Herzing, C.J. Kiely, A.F. Carley, P. Landon, G.J. Hutchings, Science 321 (2008) 1331.
[4] Z. Qu, W. Huang, M. Cheng, X. Bao, J. Phys. Chem. B 109 (2005) 15842.
[5] J. Sun, D. Ma, H. Zhang, X. Liu, X. Han, X. Bao, G. Weinberg, N. Pfänder, D. Su, J. Am. Chem. Soc. 128 (2006) 15756.
[6] H. Shinjoh, M. Hatanaka, Y. Nagai, T. Tanabe, N. Takahashi, T. Yoshida, Y. Miyake, Top. Catal. 52 (2009) 1967.
[7] Y. Nishihata, J. Mizuki, T. Akao, H. Tanaka, M. Uenishi, M. Kumura, T. Okamoto, N. Hamada, Nature 411 (2002) 164.
[8] Y. Nagai, T. Hirabayashi, K. Dohmae, N. Takagi, T. Minami, H. Shinjoh, S. Matsumoto, J. Catal. 242 (2006) 103.
[9] A.A. Newton, Chem. Soc. Rev. 37 (2008) 2644.
[10] T. Takeguchi, T. Okanishi, S. Aoyama, J. Ueda, R. Kikuchi, K. Eguchi, Appl. Catal. A 252 (2003) 205.
[11] N. Kamiuchi, H. Muroyama, T. Matsui, R. Kikuchi, K. Eguchi, Appl. Catal. A 379 (2010) 148.
[12] T. Mitsui, K. Tsutsui, T. Matsui, R. Kikuchi, K. Eguchi, Appl. Catal. B 78 (2008) 158.
[13] N. Kamiuchi, T. Matsui, R. Kikuchi, K. Eguchi, J. Phys. Chem. C 111 (2007) 16470.
[14] N. Kamiuchi, K. Taguchi, T. Matsui, R. Kikuchi, K. Eguchi, Appl. Catal. B 89 (2009) 65.
[15] N. Kamiuchi, T. Mitsui, H. Muroyama, T. Matsui, R. Kikuchi, K. Eguchi, Appl. Catal. B 97 (2010) 120.
[16] B.A.A.L. van Setten, M. Makkee, J.A. Moulijn, Catal. Rev. 43 (2001) 489.
[17] M.A. Peralta, M.S. Gross, M.A. Ulla, C.A. Querini, Appl. Catal. A 367 (2009) 59.

[18] W.F. Shangguan, Y. Teraoka, S. Kagawa, Appl. Catal. B 8 (1996) 217.
[19] A. Bueno-Lopez, K. Krishna, M. Makkee, J.A. Moulijin, J. Catal. 230 (2005) 237.
[20] J. Oi-Uchisawa, A. Obuchi, S. Wang, T. Nanba, A. Ohi, Appl. Catal. B 43 (2003) 117.
[21] M. Machida, Y. Murata, K. Kishikawa, D. Zhang, K. Ikeue, Chem. Mater. 20 (2008) 4489.
[22] A. Shigapov, A. Dubkov, R. Ukropec, B. Carberry, G. Graham, W. Chun, R. McCabe, Kinet. Catal. 49 (2008) 793.
[23] E. Aneggi, J. Llorca, C. de Leitenburg, G. Dolcetti, A. Trovarelli, Appl. Catal. B 91 (2009) 489.
[24] T. Kayama, K. Yamazaki, H. Shinjoh, J. Am. Chem. Soc. 132 (2010) 13154.
[25] K. Shimizu, H. Kawachi, A. Satsuma, Appl. Catal. B 96 (2010) 169.
[26] K. Shimizu, J. Shibata, H. Yoshida, A. Satsuma, T. Hattori, Appl. Catal. B 30 (2001) 151.
[27] C.W. Fairhurst, J.B. Cohen, Acta Cryst. B 28 (1972) 371.
[28] A. Jentys, Phys. Chem. Chem. Phys. 1 (1999) 4059.